Plastic dynamics transition between chaotic and self-organized critical states in a glassy metal via a multifractal intermediate

J. L. Ren, C. Chen, Z. Y. Liu, R. Li, and G. Wang

Phys. Rev. B **86**, 134303 — Published 12 October 2012

DOI: 10.1103/PhysRevB.86.134303

Plastic Dynamics Transition between Chaotic and Self-Organized Critical States in a Glassy Metal via a Multifractal Intermediate

J.L. Ren[1], C. Chen[1], Z.Y. Liu[2], R. Li[3], G. Wang[2,*]

[1]Department of Mathematics, Zhengzhou University, 450001 Zhengzhou, P.R. China

[2]Laboratory for Microstructures, Shanghai University, 200444 Shanghai, P.R. China

[3]School of Materials Sciences and Engineering, Beihang University, Beijing 100191, P.R. China

*Corresponding author: g.wang@shu.edu.cn

Abstract

Changes in intermittent serrated flow behavior during plastic deformation of $Zr_{64.13}Cu_{15.75}Ni_{10.12}Al_{10}$, a representative glassy metal with characteristic ductility, in response to variant strain rates and temperatures were examined. The influence of strain rates and environmental temperatures on the stress-time sequence of the plastic strain regime was investigated using comprehensive dynamical, statistical, and multifractal analyses. Three distinct spatiotemporal dynamical regimes were explored. Under small strain rates or high temperatures, the time-stress sequence exhibited a chaotic behavior. Conversely, under large strain rates or low temperatures, a transition to the self-organized critical (SOC) state was observed. In addition to chaotic time series and statistical analysis, multifractal analysis was also applied to study the crossover between these two unique plastic dynamic transitions. This plastic dynamical behavior was elucidated based on the interactions between shear avalanches in the glassy metal.

Keywords: 64.60.al; 64.60.Ht; 64.70.pe; 62.20.fk

I. Background

Serrated flow, also known as repeated yielding of glassy metals during plastic deformation, has been associated with shear band formation and propagation [1]. The shear banding processes is characterized by an accumulation of elastic energy and stress relaxation accompanied by adiabatic heating [2]. Various physical parameters and models have been deduced to quantitatively describe the ductility of glassy metals [3-8] in the framework of continuum theory [9,10]. A phenomenological model, or testing machine-sample system, was schematically designed for the purpose of serration event elucidation [11]. Furthermore, the lack of periodicity in intermittent serrated flow has necessitated statistical analysis to extract hidden information from these serration events [12-15]. The results of such studies suggest that glassy metals with different ductilities may present two distinct dynamical behaviors, a self-organized critical (SOC) behavior and a chaotic behavior [12,13]. The mechanism of the transition between these two behaviors, however, has not been documented.

Analysis of dynamic behaviors in crystalline materials has revealed several common stress serration types. Additionally, observations of distinct deformation band patterns in various materials have been linked to certain experimental conditions, such as temperatures and mechanical treatments [14]. Based on determination of their characteristics, instabilities of plastic flow at different applied strain rates can be classified into three primary categories: SOC behavior, chaotic behavior, and random nucleation. The SOC behavior is characterized by the continuous propagation of deformation bands near the upper strain rate boundary of plastic instability. At lower strain rates, successive formation of distinct and adjacent deformation bands is described as chaotic behavior [14]. Throughout the range of intermediate strain rates, these bands are thought to nucleate

randomly, which remains a missing connection between SOC and the chaotic behavior in glassy metals.

In order to provide clear evidence of the mechanism occurring at intermediate stages between SOC and chaotic behaviors, a multifractal analysis [15] of the stress-time series in the serrated flow was conducted in order to identify spatial and temporal shear avalanches in a glassy metal. The purpose of the present study was not only to provide an improved understanding of this intriguing spatiotemporal behavior but also to define the detrimental influence of the serrated flow behavior on the mechanical properties of glassy metals. The glassy metal $Zr_{64.13}Cu_{15.75}Al_{10}Ni_{10.12}$ was selected as the representative model material due to its significant ductility at the room temperature [16]. Through modification of environmental temperatures and loading rates, the plastic stress-strain response of this glassy metal was investigated by statistical, dynamical, and multifractal analysis.

II. Experimental procedure

Alloy ingots of the glassy metal $Zr_{64.13}Cu_{15.75}Al_{10}Ni_{10.12}$ were prepared by arc melting a mixture of pure metal elements (purity >99.99%) in a titanium-gettered argon atmosphere. This treatment was immediately followed by suction casting into copper moulds to form rod-like samples with a size of Φ2×70 mm. Compressive test specimens were fabricated from these rod-like glassy metal samples by means of a diamond saw using water as a coolant, resulting in test specimens with a height of 4 mm and a diameter of 2 mm.

Compressive tests were conducted using a legacy dynamics and fatigue system model 8562 electric-actuator (Instron) equipped with an environmental box with three strain rates, 2.5×10^{-2} s^{-1}, 2.5×10^{-3} s^{-1}, and 2.5×10^{-4} s^{-1}. The temperature accuracy of the environmental box maintained at ± 2 K. To exclude the influence of data acquisition frequency on stress fluctuation sensitivity, data

acquisition frequencies of 0.5, 1.0, 10.0, and 100.0 point/s with increasing strain rate were selected. After fracture, the surface of specimens were observed by a JEOL JSM-6335F scanning electron microscope (SEM).

III. Results

At cryogenic temperature, the extensometer cannot directly yield accurate strain values. Thus, compressive nominal stress-time (σ-t) curves were plotted to reflect the elasto-plastic behavior of $Zr_{64.13}Cu_{15.75}Al_{10}Ni_{10.12}$. Figure 1(a) shows the comparative plot of the σ-t curves at different temperatures at a common strain rate of 2.5×10^{-3} s^{-1}, demonstrating linear elastic deformation followed by a plastic flow plateau. Temperature reduction induces both yield strength and plasticity in the glassy metal, consistent with previous findings [1,17,18]. The strain rate, however, does not significantly influence the mechanical properties of the glassy metal. The compression deformations at 293 K with different strain rates are representatively shown in Figs. 1(a), (b), and (c).

The variation in serration events in the plastic regime of the glassy metal achieved by varying temperature and strain rate can be characterized by observing the plastic regime near the fracture region, as shown in Fig. 2. It is evident that the amplitude of the serration event decreases with decreasing temperature, as shown in Figs. 2(a), (c), and (e). At 293 K, the amplitude of the serration event was approximately 25 MPa [Fig. 2(a)]. When the temperature was reduced to 213 K, the amplitude of the serration event decreased to approximately 5 MPa [Fig. 2(e)]. The serration event was completely obscured as temperature continued to decrease. Stress fluctuations resulting from machine vibrations and sample to cross-head friction are the primary events obscuring the amplitude of the serration events (not shown). Increasing strain rates also highlight the decreased serration event amplitude [Figs. 2(a), (g) and (i)]. Strain rate increases from ~10^{-4} s^{-1} to ~10^{-2} s^{-1}

result in stress amplitude reduction from ~25 MPa to ~7 MPa.

After fracture, numerous shear bands can be observed on the surface of glassy metals deformed at different strain rates and temperatures. Figure 3 comparatively shows the lateral surface morphologies of the fractured glassy metal under three test conditions, demonstrating that all specimens exhibit shear facture [Fig. 3; see insets]. With increased strain rate and decreased temperature, a larger number of shear bands were apparent on the glassy metal surface compared with the number observed at the strain rate of 10^{-4} s^{-1} and the temperature of 293 K [Figs. 3(b) and (c); arrows indicate banding]. These findings are consistent with previous results [17,18].

IV. Discussion

The hidden information apparent in the stress-time response of the glassy metal at different temperatures and strain rates can be determined by dynamic analysis, allowing for further characterization of the stress-time sequence: $\{\sigma(t), (t = 1, 2,\ldots\ldots, N)\}$, where $\sigma(t)$ is the stress at the time of t (Figs. 1 and 2). The range of the stress-time sequence in each stress-time curve is from the yield strain to fracture strain. Accurate deterministic dynamical system modeling relies on the phase space concept and the collection of possible system states. As an experimentally occurring dynamical system, the phase space and mathematical description of the plastic dynamical system in the glassy metal are unknown. A phase space reconstruction for the stress-time sequence of $\{\sigma(t), (t = 1, 2,\ldots\ldots, N)\}$ is required to build a proxy of the observed states, as previously described [19]. Because the mathematical model of the unknown chaotic dynamical system has equivalent geometrical characteristics with the reconstructed m-dimensional phase space, the original chaotic dynamics can be studied through reconstruction of the phase space.

After selecting an appropriate time delay (τ) by the mutual information method [20] and

calculating the embedding dimension (m) by the Cao-method [21], the stress-time sequence $\{\sigma(t), (t = 1, 2,\ldots\ldots, N)\}$ can be transformed into a set of $\{Y(t_i), (t_i = 1, 2,\ldots\ldots, [N\text{-}(m\text{-}1)])$ constituting a m-dimension vector of $Y(t_i) = \{\sigma(t_i), \sigma(t_i+\tau),\ldots\ldots, \sigma(t_i+(m\text{-}1)\tau)\}$. Following this transformation, the reconstructed m-dimension phase space may be constructed. The delay time, τ, and the embedding dimension, m, changing with the strain rates and the temperatures are listed in Tables I and II, respectively. Then, according to these values, take an initial point $Y(t_0)$ and its nearest neighbor point $Y(t_0^*)$ in the reconstructed phase space, and denote $Y_0 = Y(t_0^*) - Y(t_0)$. After a period of time, the points $Y(t_0)$ and $Y(t_0^*)$ will transit to $Y(t_1)$ and $Y(t_1^*)$, correspondingly, and then denote $Z_0 = Y(t_1^*) - Y(t_1)$. By means of the least squares method, the matrix, A_0 can be constructed to map the evolution from Y_0 to Z_0, where $Z_0 = A_0 Y_0$. By repeating the above steps from $Y(t_1)$ to $Y(t_2)$ and so forth, a list of A_i (where $i = 1, 2,\ldots\ldots, p$) can be calculated. By applying a standard QR decomposition for the matrix A_i, where $A_i = Q_i R_i$, the Lyapunov exponent spectrum can be determined: $\lambda_k = \frac{1}{t_{p-1} - t_0} \sum_{i=0}^{p} \ln(R_i)_{kk}$, where $k = 1, 2, ,\ldots\ldots, m$. Note that different Lyapunov exponents of the dynamic system are achieved under different deformation conditions. If the largest Lyapunov exponent is negative, the two adjacent points in the dynamical system will be convergent (corresponding to a stable state). Conversely, if the largest Lyapunov exponent is positive, then the two adjacent points will separately evolve (The Butterfly Effect), representative of chaotic dynamics.

The largest Lyapunov exponents observed during the deformation of the glassy metal at different temperatures and strain rates are listed in Tables I and II, respectively. The largest Lyapunov magnitude of exponent variation from positive to negative occurred as the strain rate increased from 2.5×10^{-4} s^{-1} to 2.5×10^{-2} s^{-1} and as the temperature decreased from 293 K to 213 K. Thus, it is clear that higher temperatures and lower strain rates are associated with larger positive

Lyapunov exponents, suggesting the occurrence of chaotic dynamic behavior.

The above stress-time sequence uses the largest Lyapunov exponent to characterize the chaotic behavior (instable state). According to previous results from studies of single crystals [22], polycrystals [23], and nanocrystals [24,25], large negative Lyapunov exponents (stable state) are indicative of SOC behavior in the serrated flow. Thus, further statistical analysis of the stress drop occurring during each serration event in the current plastic flow are necessary.

The enlarged stress-time curves shown in the left column of Fig. 2 represent the transition in serration events with temperature and strain rates. The corresponding quantity $|d\sigma/dt|$ clearly reflects bursts of plastic activity (Fig. 2; right column). The $|d\sigma/dt|$ value as the function of time (t) shows that this burst of plasticity exhibits roughly same periodicity (time intervals; t_{n-1}, t_n, t_{n+1}) between any two neighboring serration events. Thus, these events are homogeneous ($t_{n-1} \approx t_n \approx t_{n+1}$) at low strain rates ($2.5\times10^{-4}$ s^{-1} and 2.5×10^{-3} s^{-1}) and relatively high temperatures (293 K and 223 K) [Figs. 2(b), (d), and (h)]. Decreasing the temperature to 213 K or increasing the strain rate to 2.5×10^{-2} s^{-1} causes inhomogeneous ($t_{n-1} \neq t_n \neq t_{n+1}$) time intervals ($t_n$) to appear [Figs. 2(f) and (j)], suggesting that serration events at relatively lower temperatures (< 213 K) or higher strain rates (> 10^{-2} s^{-1}) lack any typical time scale. This finding is characteristic of SOC behavior [26].

Therefore, by referring to the largest Lyapunov exponents in Table I and II, the inhomogeneous time interval distributions and largest negative Lyapunov exponents suggest the possible occurrence of SOC behavior at low temperatures and high strain rates. To confirm this finding, the statistical distribution of the stress drop size of serration events was investigated [Fig. 2(a)]. The plastic flow of glassy metals has been previously shown to be dominated by shear avalanches [27]. From the stress-time curves (Fig. 1 and 2), a stress drop ($\Delta\sigma$) can be constructed to characterize the elastic energy relaxation process. This construct can also reflect the shear avalanche length of each

serration event [10]. Noise influences have been shown to cause small serrations in the elastic stage that emerge during the plastic deformation stage [10]. Due to this effect, the serration events were removed before the stress drop reached 2 MPa, as deduced by linear fitting of the elastic regime in the stress-time curve (not shown), prior to statistical analysis of the stress drops [12]. Since plastic strain results in drift of the stress drop value, stress drop normalization was carried out to eliminate statistical error [12]. Through linear regression fitting, the plot of stress drop versus time baseline [$f(t)$] was obtained. The statistical distribution of the normalized stress drop is given as: $S(\Delta\sigma) = \Delta\sigma/f(t)$, where $S(\Delta\sigma)$ is the probability density at the stress drop of $\Delta\sigma$ (Fig. 4). Peak distributions are observed in chaotic behaviors, such as the plastic deformation occurring at temperatures of 293 K and 223 K and strain rates of 10^{-4} s^{-1} and 10^{-3} s^{-1} [Figs. 4(a), (b), (d), and (f)]. At higher strain rates ($> 10^{-2}$ s^{-1}) and lower temperatures (< 213 K), the statistical distribution of the stress drop values evidence a monotonic decrease [Figs. 4(c), and (e)]. These distributions eventually lead to a power-law relation: $S(\Delta\sigma) \sim \Delta\sigma^{-\alpha}$ [Figs. 4(c) and (e); insets]. The stress drop generates a shear band pattern following a fractal structure [28], characteristic of a power-law relation. These observations indicate that shear banding may self-organize to a critical state [12]. Thus, a power-law distribution of the shear avalanche will occur spatiotemporally [29], further suggesting a dynamic behavior transition to the SOC state as the temperature decreases or strain rate increases [14].

Due to the lack of periodic structure, the ductility of the glassy metal is governed by shear banding rather than by the motion of crystalline defects [30]. Furthermore, this shear banding is likely to be associated with the serration event [10]. Before shear banding occurs, an elastic strain field forms in the elastic energy accumulation regime of each serration event [31]. The size of this elastic strain field is approximately 500 μm, a value much larger than the 100 μm inter-space between neighboring shear bands (d) [Fig. 3(a); cf.]. This indicates interference between

neighboring elastic strain fields. As stress drops during serration events, elastic energy is relaxed and the elastic strain field subsequently disappears. In higher strain rate ranges ($>10^{-2}$ s^{-1}), energy accumulation time decreases and becomes equivalent to relaxation time (t_l / $t_r \approx \sim 1$) [Table III; cf.], suggesting failure of the elastic strain field to totally relax during this limited time. This promotes the formation of new shear bands adjacent to existent bands in the temporal space. Thus, new shear bands are formed in the field of the unrelaxed elastic strain field. Overlap in the elastic strain field can result in a hierarchy of length scales [14], leading to SOC behavior. At lower strain rates, such as 10^{-4} s^{-1}, energy accumulation time (t_l) is approximately 40 times larger than relaxation time (t_r) (Fig. 2; Table III). At this strain rate, the elastic strain field can be fully relaxed, and no spatial correlation between shear bands is apparent. This is characteristic of chaotic behavior.

Dynamic propagation of the shear band is associated with shear transformation zones (STZs). STZs are usually formed in the plastic zone in front of the shear band tip [32]. Also, STZ formation and assembly results in shear banding. As the environmental temperature decreases to the cryogenic temperature, the size of STZs will expand [17]. This observation indicates that the creation of STZs requires higher activation energies [5]. Thus, the propagation of shear bands may become more difficult at the cryogenic temperature. The frozen propagation of shear bands may thus facilitate the nucleation of an increasing number of subsidiary shear bands, as observed by direct observation of specimen surfaces [Fig. 3(c); cf.]. These subsidiary shear bands are characterized by small serration events (Fig. 2). The decreased amplitude of these serration events corresponds to temperature decreases and dispersal of elastic energy. Cumulatively, these findings indicate that the system exhibits a dynamic transition between the chaotic state and the SOC state at intermediate temperatures and strain rates.

In the glassy metal, a plastic dynamic transition from SOC to chaotic behavior was observed

with decreasing strain rate or increasing temperature. The boundary between these two dynamical behaviors, however, remains unclear. To clarify this issue, a multi-fractal analysis was applied to study the crossover of the plastic dynamics transition [14].

The stress burst sequence was defined as: $\psi_t = \{|d\sigma/dt|,\ t = 1, 2, \ldots\ldots, K\}$ (Fig. 2). This sequence can be divided by time scales (Δt) into time intervals: $N = N(\Delta t)$. Each time interval includes m points. The probability in the i^{th} time interval is measured by: $p_i(\Delta t) = \sum_{k=1}^{m} \psi_{im+k} / \sum_{j=1}^{K} \psi_j$. A scale-less band exhibits $p_i(\Delta t) \sim \Delta t^{\alpha}$, where the exponent α is the singularity strength. At different i values, a series of α can be obtained. Denote the range of multifractal spectrum by $\Delta\alpha = \alpha_{\max} - \alpha_{\min}$, which reflects the probability distribution of the whole fractal structure. If $\Delta\alpha$ is equal to zero (in theory) or small enough to approach to zero, the uniformity of the probability distribution suggests that a single fractal exists. Conversely, if $\Delta\alpha$ is relatively large compared to the value in the single fractal case, nonuniformity indicates a multifractal state. The multifractal spectrum may be calculated using the previously described partition function method [33]. If $N_\alpha(\Delta t)$ is the number of time intervals (Δt) with singularity strength α, then $N(\Delta t)$ generalizes to $N_\alpha(\Delta t) \sim \Delta t^{-f(\alpha)}$, where $f(\alpha)$ is the singularity spectrum. This reflects the fractal dimension of the subset characterized by the singularity strength α. If the partition function is defined as $\chi_q(\Delta t) = \sum_i p_i^q$, where q is the weighting factor, the fractal scale-less band exhibits the following scale relations: $\chi_q(\Delta t) \sim \Delta t^{\tau(q)}$, where $\tau(q)$ is the scaling exponent. Then, $\alpha, f(\alpha)$ can be evaluated by $\alpha(q) = \frac{d\tau(q)}{dq}$ and $f(\alpha) = q \cdot \alpha(q) - \tau(q)$, a Legendre transformation.

The multi-fractal spectrum $[\alpha, f(\alpha)]$ for the temperature 253 K at the strain rate 2.5×10^{-4} s^{-1} and the temperature 293 K at the strain rate 2.5×10^{-3} s^{-1} are shown in Figures 5(a) and (b), respectively. Figure 6(a) shows a multifractal range of $\Delta\alpha$ as the temperature increases from 203 K to 293 K, at a

strain rate of ~10^{-4} s^{-1}. The largest $\Delta\alpha$ value is observed at intermediate temperatures, indicating a multifractal burst. At a constant temperature of 293 K and an increasing strain rate from 2.5×10^{-4} s^{-1} to 2.5×10^{-2} s^{-1}, a peak $\Delta\alpha$ value also appears in the transition stage [Fig. 6(b)]. This finding indicates a multifractal burst at the strain rate of 2.5×10^{-3} s^{-1}. Figures 6(a) and (b) illustrate multifractal bursts in the transition region of the spatiotemporal dynamics of the serrated flow. The plastic dynamics of the glassy metal transition from a disordered state (chaotic state) to an intermediate state (multifractal state) and finally to an ordered state (SOC state) are shown to correlate with increasing strain rates and decreasing temperatures.

V. Conclusions

Chaotic time series analysis, statistical analysis, and multifractal analysis studies indicated that the plastic dynamics of $Zr_{64.13}Cu_{15.75}Ni_{10.12}Al_{10}$, a representative glassy metal, are characterized by a transition from the chaotic state to the SOC state through an intermediate multifractal state. This transition was shown to be correlated with both increasing strain rates and decreasing temperatures. Furthermore, the intermediate state was characterized by the presence of multifractal bursts, and disorderly shear branches were observed at small strain rates. With increasing strain rates and decreasing temperatures, however, interactions between shear branches were implicated in the formation of a multifractal structure. The final result of this plastic dynamic behavior is the transition to a self-organized state with a complete fractal structure. This represents a natural transition between the disordered and ordered stages in glassy metals.

Acknowledgements

The work described in this paper is supported by the NSF of China (Nrs. 11271339, 51171098 and 51222102) and the NCET (10-0141) program. G. W. also thanks the financial support by

Shanghai Pujiang Program (Nr. 11PJ1403900), and the Program for Professor of Special Appointment (Eastern Scholar) at Shanghai Institutions of Higher Learning.

References

[1] D. Klaumünzer, A. Lazarev, R. Maaß, F.H. Dalla Torre, A. Vinogradov, and J.F. Löffler, Phys. Rev. Lett. **107**, 185502 (2011).

[2] J.J. Lewandowski, and A.L. Greer, Nat. Mater. **5**, 15 (2006).

[3] J.J. Lewandowski, W.H. Wang, and A.L. Greer. Philo. Mag. Lett. **85**, 77 (2005).

[4] J. Schroers, and W.L. Johnson. Phys. Rev. Lett. **93,** 255506 (2004).

[5] D. Pan, A. Inoue, T. Sakurai, and M.W. Chen, Proce. National. Am. Soc. **105**, 14769 (2008).

[6] F. Spaepen, Acta Metall. **25**, 407 (1977).

[7] Y.H. Liu, D. Wang, K. Nakajima, W.Zhang, A. Hirata, T. Nishi, A. Inoue, and M.W. Chen, Phys. Rev. Lett. **106**, 125504 (2011).

[8] W.L. Johnson, and K. Samwer, Phys. Rev. Lett. **95**, 195501 (2005).

[9] A. Portevin, and F. Le Chatelier, C. R. Acad. Sci. **176**, 507 (1923).

[10] G. Wang, K.C. Chan, L. Xia, P. Yu, J. Shen, and W.H. Wang, Acta Mater. **57**, 6146 (2009).

[11] Y.Q. Cheng, Z. Han, Y. Li, and E. Ma, Phys. Rev. B **80**, 134115 (2009).

[12] B.A. Sun, H.B. Yu, W. Jiao, H.Y. Bai, D.Q. Zhao, and W.H. Wang, Phys. Rev. Lett. **105**, 035501 (2010).

[13] R. Sarmah, G. Ananthakrishna, B.A. Sun, and W.H. Wang, Acta Mater. **59**, 4482 (2011).

[14] M.S. Bharathi, M. Lebyodkin, G. Ananthakrishna, C. Fressengeas, and L.P. Kubin, Phys. Rev. Lett. **87**, 165508 (2001).

[15] M.A. Lebyodkin, and T.A. Lebedkina, Phys. Rev. E **77**, 026111 (2008).

[16] Y.H. Liu, G. Wang, R.J. Wang, D.Q. Zhao, M.X. Pan, and W.H. Wang, Science **315**, 1385 (2007).

[17] D. Pan, H. Guo, W. Zhang, A. Inoue, and M.W. Chen, Appl. Phys. Lett. **99**, 241907 (2011).

[18] H.Q. Li, C. Fan, K.X. Tao, H. Choo, and P.K. Liaw, Adv. Mater. **18**, 752 (2006).

[19] S.H. Strogatz, Nonlinear Dynamics and Chaos (MA: Perseus Books, Cambridge, 1994).

[20] A.M. Fraser, and H.L. Swinney, Phys. Rev. A **33**, 1134 (1986).

[21] L. Cao, Physica D: Nonlinear Phenomena **110**, 43 (1997).

[22] M.C. Miguel, A. Vespignani, S. Zapperi, J. Weiss, and J.R. Grasso, Nature (London) **410**, 667 (2001).

[23] T. Richeton, J. Weiss, and F. Louchet, Nature Mater **4**, 465 (2005).

[24] D.M. Dimiduk, C. Woodard, R. Lesar, and M.D. Uchic, Science **312**, 1188 (2006).

[25] F.F. Csikor, C. Motz, D. Weygand, M. Zaiser, and S. Zapperi, Science **318**, 251 (2007).

[26] M. Koslowski, R. LeSar, and R. Thomson, Phys. Rev. Lett. **93**, 125502 (2004).

[27] J.L. Ren, C. Chen, G. Wang, N. Mattern, and J. Eckert, AIP Advances **1**, 032158 (2011).

[28] B.A. Sun, and W.H. Wang, Appl. Phys. Lett. **98**, 201902 (2011).

[29] B.A. Sun, S. Pauly, J. Tan, M. Stoica, W.H. Wang, U. Kühn, and J. Eckert, Acta Mater. **60**, 4160 (2012).

[30] G. Wang, X. H. Xu, F. J. Ke, and W. H. Wang, J. Appl. Phys. **104**, 073530 (2008).

[31] J.W. Qiao, A.C. Sun, E.W. Huang, Y. Zhang, P.K. Liaw, and C.P. Chuang, Acta Mater. **59**, 4126 (2011).

[32] W.J. Wright, M.W. Samale, T.C. Hufnagel, M.M. LeBlanc, and J.N. Florando, Acta Mater. **57**, 4639 (2009).

[33] X. Sun, Z.Q. Wu, and Y. Tian, Fractal Method and Applications (University of Science and Technology of China Press, 2006).

Figure captions

Fig. 1 Nominal stress-time curves of the $Zr_{64.13}Cu_{15.75}Al_{10}Ni_{10.12}$ glassy metal at different temperatures and strain rates. (a) Comparative stress-time curves deformed at three temperatures. (b) Stress-time curve deformed at a temperature of 293 K and strain rate of $\sim 10^{-4}$ s^{-1}. (c) Stress-time curve deformed at a temperature of 293 K and strain rate of $\sim 10^{-2}$ s^{-1}.

Fig. 2 Enlarged stress-time curves of the $Zr_{64.13}Cu_{15.75}Al_{10}Ni_{10.12}$ glassy metal at different temperatures and strain rates, along with a plot of the corresponding $|d\sigma/dt|$ curves. *Note*: t_n indicates the processing time of one serration event.

Fig. 3 Surface morphologies of the fractured $Zr_{64.13}Cu_{15.75}Al_{10}Ni_{10.12}$ glassy metal at different temperatures and strain rates. (a) Fracture at a strain rate of $\sim 10^{-4}$ s^{-1} and temperature of 293 K. (b) Fracture at strain rate of $\sim 10^{-2}$ s^{-1} and temperature of 293 K. (c) Fracture at strain rate of $\sim 10^{-4}$ s^{-1} and temperature of 213 K.

Fig. 4 Statistic distribution of stress drop [$S(\Delta\sigma)$] of the $Zr_{64.13}Cu_{15.75}Al_{10}Ni_{10.12}$ glassy metal deformed at different temperatures and strain rates. The power-law distribution of the stress drop is indicated in the inset.

Fig. 5 (a) Multi-fractal spectrum $(\alpha, f(\alpha))$ for the temperature 253 K at the strain rate 2.5×10^{-4} s^{-1}: $q \in [-5,+5]$. (b) Multi-fractal spectrum $(\alpha, f(\alpha))$ for the temperature 293 K at the strain rate 2.5×10^{-3} s^{-1}: $q \in [-5,+5]$.

Fig. 6 (a) Range of multifractal spectrum $\Delta\alpha$ vs. the temperature at a strain rate of $\sim 10^{-4}$ s^{-1}. (b) Range of multifractal spectrum $\Delta\alpha$ vs. applied strain rate at a temperature of 293 K.

Table I The time delay, τ, the embedding dimension, m, and the largest Lyapunov exponents, λ_1, vs. strain rate at temperature of 293 K.

Strain rate (s^{-1})	2.5×10^{-4}	2.5×10^{-3}	2.5×10^{-2}
τ	4	28	4
m	7	7	6
λ_1	0.268	0.002	-0.003

Table II The time delay, τ, the embedding dimension, m, and the largest Lyapunov exponents, λ_1, vs. the temperature at strain rate of $\sim10^{-4}$ s^{-1}.

Temperature (K)	293	273	253	223	213
τ	4	14	11	33	26
m	7	10	8	10	8
λ_1	0.268	0.198	0.050	0.002	-0.0008

Table III The elastic accumulation time (t_l) and the stress relaxation time (t_r) in serration events at different strain rates and temperatures.

Strain rate (s^{-1})	Temperature (K)	t_l (s)	t_r (s)	t_l / t_r
10^{-4}	293	~4.321	~0.122	~40
10^{-4}	273	~2.853	~0.121	~30
10^{-4}	253	~2.374	~0.123	~20
10^{-4}	223	~1.322	~0.364	~4
10^{-4}	213	~0.813	~0.392	~2
10^{-3}	293	~0.244	~0.096	~3
10^{-2}	293	~0.020	~0.022	~1

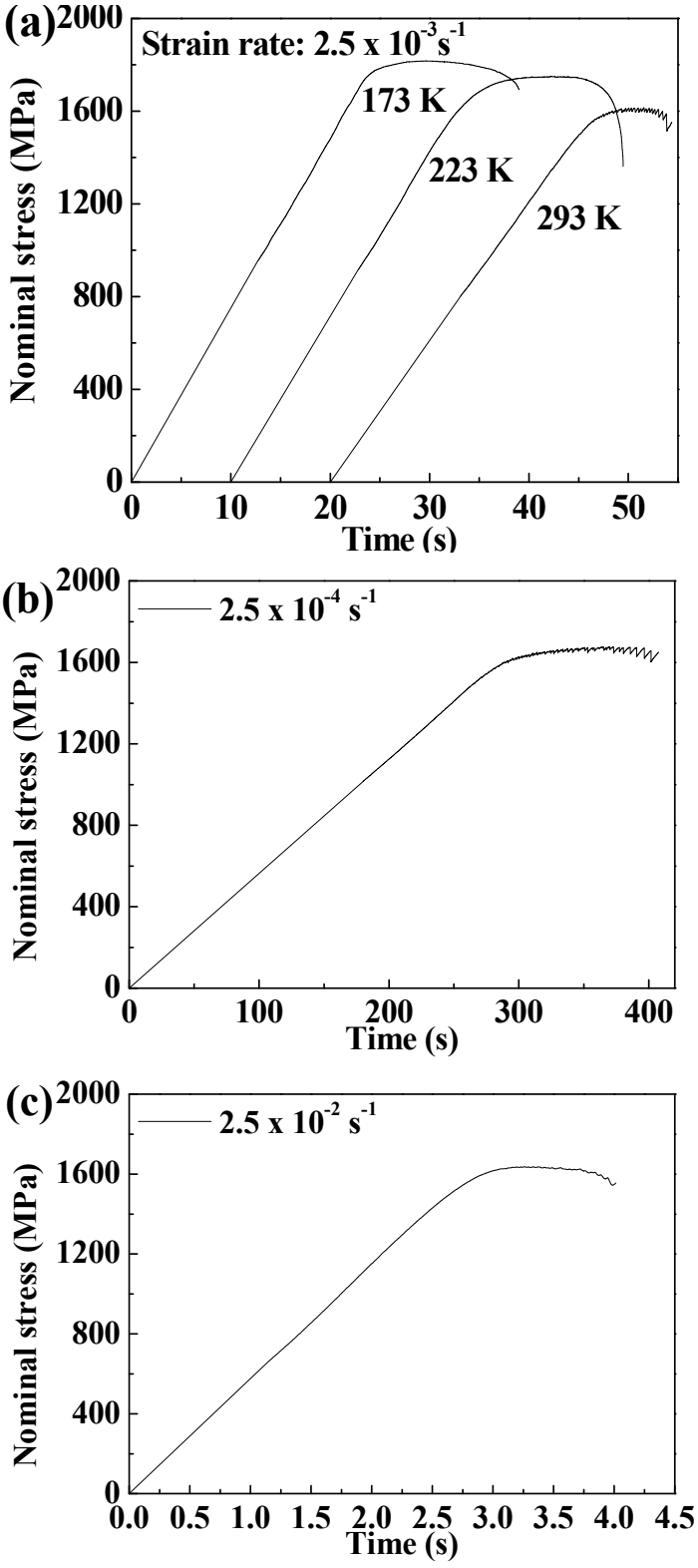
(a)
Strain rate: 2.5 x 10^-3 s^-1
173 K
223 K
293 K
Nominal stress (MPa)
Time (s)
(b)
2.5 x 10^-4 s^-1
Nominal stress (MPa)
Time (s)
(c)
2.5 x 10^-2 s^-1
Nominal stress (MPa)
Time (s)

Fig. 1

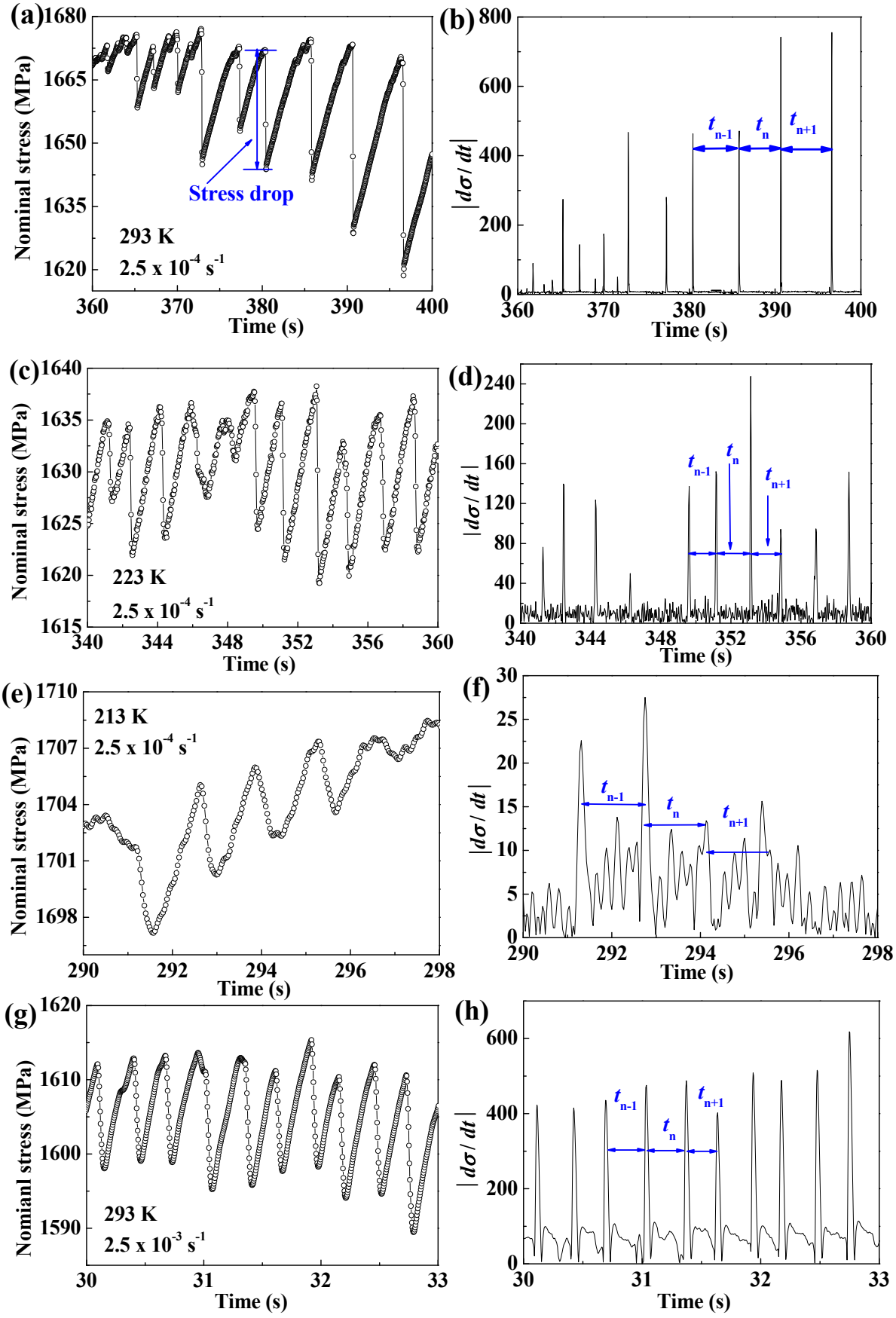
(a)
Nominal stress (MPa)
Time (s)
Stress drop
293 K
2.5 x 10^-4 s^-1
(b)
|dσ/dt|
t_n-1
t_n
t_n+1
Time (s)
(c)
Nominal stress (MPa)
223 K
2.5 x 10^-4 s^-1
Time (s)
(d)
|dσ/dt|
t_n-1
t_n
t_n+1
Time (s)
(e)
Nominal stress (MPa)
213 K
2.5 x 10^-4 s^-1
Time (s)
(f)
|dσ/dt|
t_n-1
t_n
t_n+1
Time (s)
(g)
Nomianl stress (MPa)
293 K
2.5 x 10^-3 s^-1
Time (s)
(h)
|dσ/dt|
t_n-1
t_n
t_n+1
Time (s)

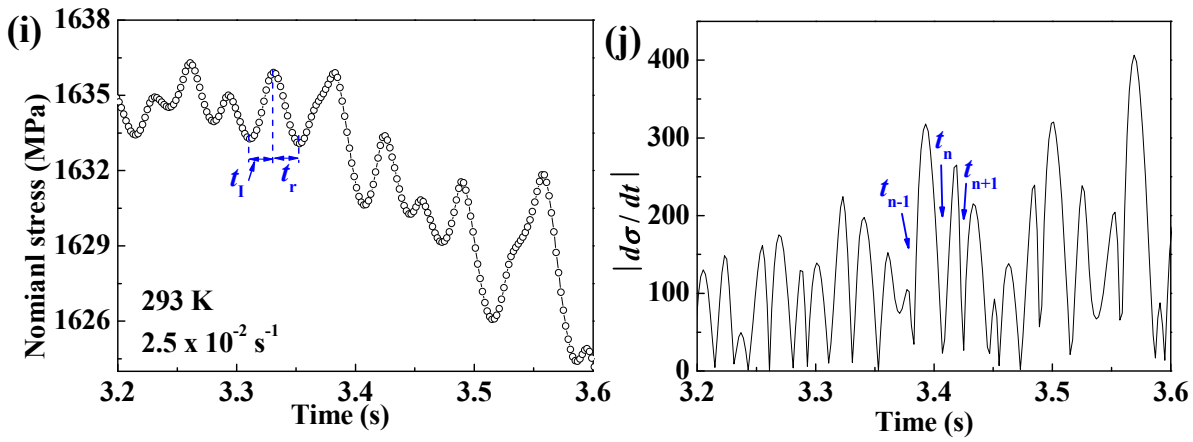
(i)
Nomianl stress (MPa)
1638
1635
1632
1629
1626
293 K
2.5 x 10^-2 s^-1
t_l
t_r
3.2
3.3
3.4
3.5
3.6
Time (s)
(j)
|dσ/dt|
400
300
200
100
0
t_n-1
t_n
t_n+1
3.2
3.3
3.4
3.5
3.6
Time (s)

Fig. 2

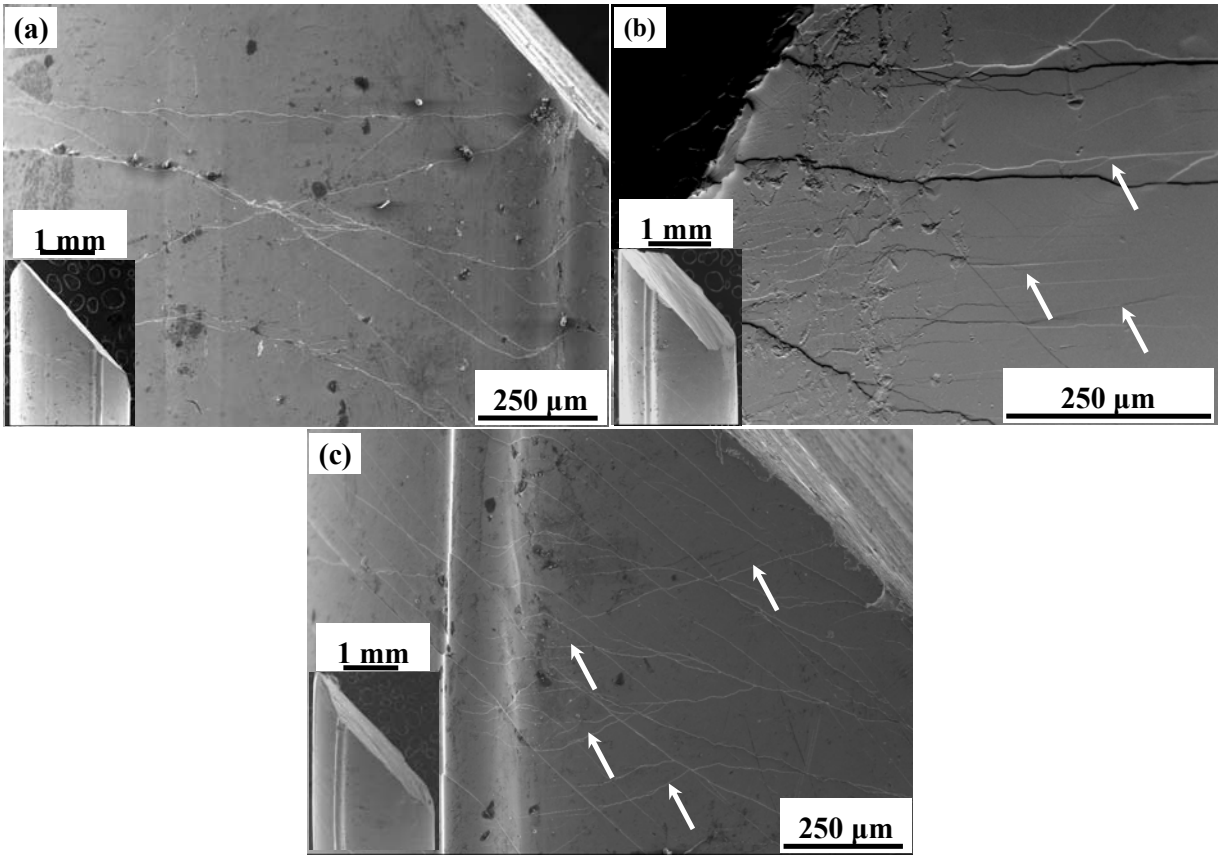

Fig. 3

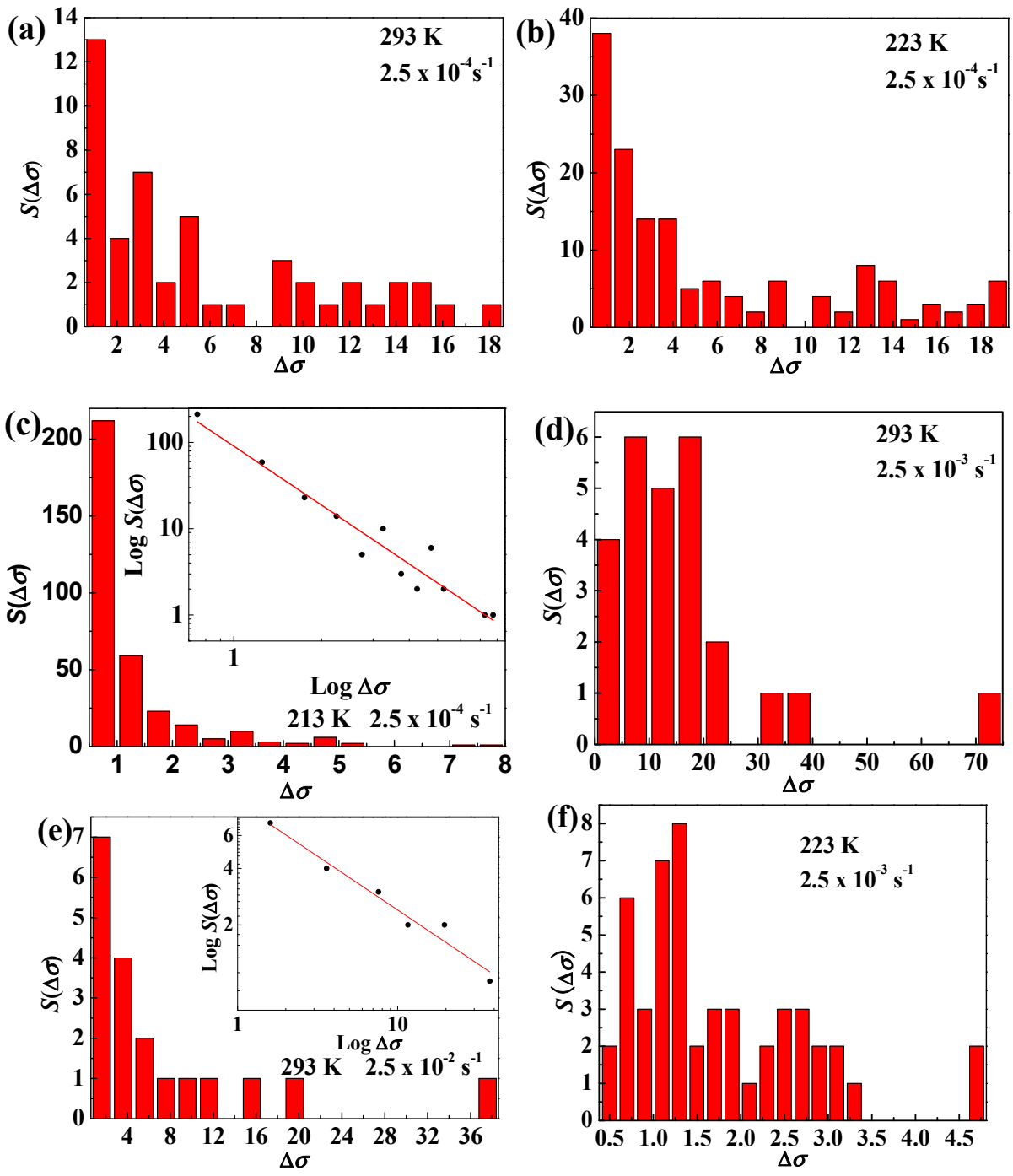
(a)
293 K
2.5 x 10^-4 s^-1
S(Δσ)
Δσ
(b)
223 K
2.5 x 10^-4 s^-1
S(Δσ)
Δσ
(c)
Log S(Δσ)
Log Δσ
213 K 2.5 x 10^-4 s^-1
S(Δσ)
Δσ
(d)
293 K
2.5 x 10^-3 s^-1
S(Δσ)
Δσ
(e)
Log S(Δσ)
Log Δσ
293 K 2.5 x 10^-2 s^-1
S(Δσ)
Δσ
(f)
223 K
2.5 x 10^-3 s^-1
S (Δσ)
Δσ

Fig. 4

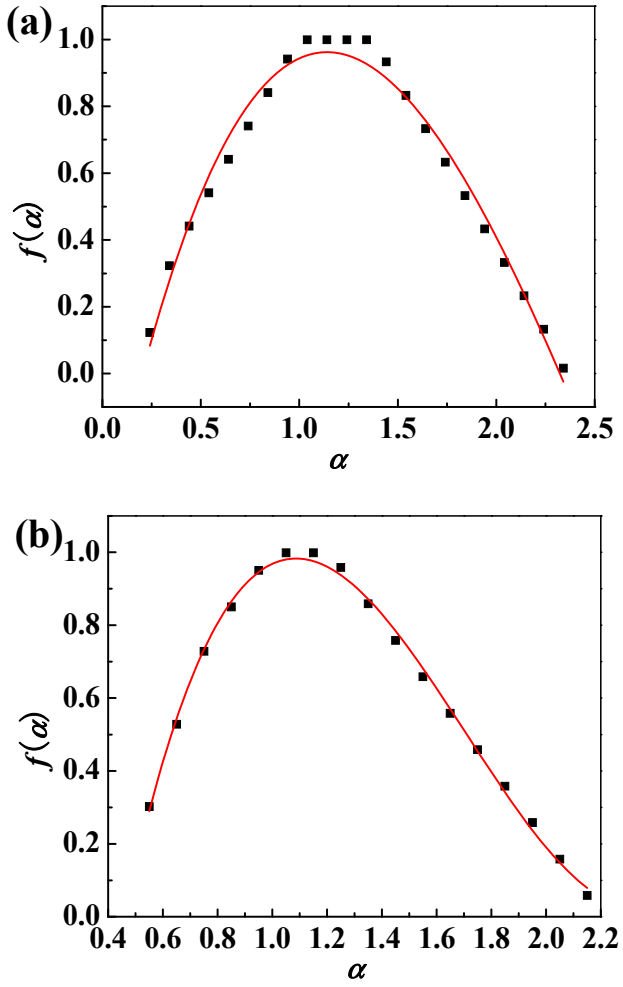
(a)
1.0
0.8
0.6
0.4
0.2
0.0
f(α)
0.0
0.5
1.0
1.5
2.0
2.5
α
(b)
1.0
0.8
0.6
0.4
0.2
0.0
f(α)
0.4
0.6
0.8
1.0
1.2
1.4
1.6
1.8
2.0
2.2
α

Fig. 5

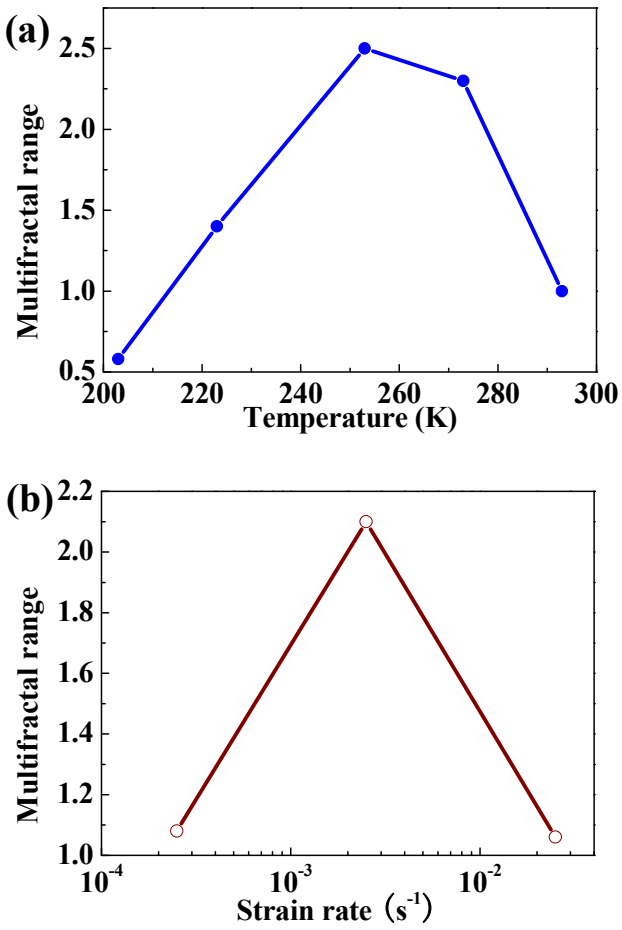
(a)
Multifractal range
2.5
2.0
1.5
1.0
0.5
200
220
240
260
280
300
Temperature (K)
(b)
Multifractal range
2.2
2.0
1.8
1.6
1.4
1.2
1.0
10-4
10-3
10-2
Strain rate (s-1)

Fig. 6